International Journal of Mechanical Sciences 131–132 (2017) 305–316

Contents lists available at ScienceDirect

International Journal of Mechanical Sciences

journal homepage: www.elsevier.com/locate/ijmecsci

Contact stiffness of multiscale surfaces by truncation analysis

Chongpu Zhai [a], Dorian Hanaor [a,b], Yixiang Gan [a,*]

[a] School of Civil Engineering, The University of Sydney, Sydney, Australia
[b] Institute for Material Science and Technologies, Technical University of Berlin, Berlin, Germany

ARTICLE INFO

Keywords:
Contact stiffness
Rough surfaces
Fractal dimension
Nanoindentation

ABSTRACT

In this paper, we study the contact stiffness of a fractal rough surface compressed by a rigid flat plane. A numerical model based on the analysis of flat punch indentation is proposed for simulated hierarchical surfaces, which are generated using statistical and fractal descriptors collected by surface profilometry. The contact stiffness of surfaces under increasing normal load is determined on the basis of the total truncated area at varying heights. The results are compared with experimental data from nanoindentation on four types of treated rough surfaces, showing good agreement with experimental observations below a certain truncation depth. Furthermore, the limits of the model's validity are discussed by focusing on surface geometries and deformation of contacting asperities. With this proposed truncation method, we present a parametric analysis to establish a correlation between contact stiffness and surface roughness descriptors. The contact stiffness shows a unified power-law scaling with respect to the applied load over a wide range for simulated surfaces with distinct sets of roughness descriptors. The exponent of the power-law relationship is found to correlate positively to the fractal dimension while its amplitude is inversely correlated to the surface roughness amplitude. This study provides an easily implemented and computationally efficient method to connect mechanical behaviour with multi-scale surface structure, which can be utilized in design and optimization of engineering applications involving rough contacts.

1. Introduction

The morphology of surfaces plays a determining role in interfacial phenomena including friction, adhesion, sealing, lubrication and thermal and electrical conductance [1,2]. When two solids with rough surfaces are squeezed together, the area of true contact consists of numerous contact patches of various sizes and generally comprises only a small fraction of the nominal contact area. Over the years, numerous divergent approaches have been developed to explore load dependent contact behaviour at rough surfaces, yet the scientific community remains divided regarding the reliability of their predictions [1,3–6]. The various asperity-based approaches to contact models reported in the literature can be categorized as: (1) multi-asperity contact models (i.e., statistical models), in which the heights and / or curvatures of asperities follow given statistical distributions [7–10]; and (2) surface fractality models, including multi-scale models [11–17], the boundary element method (BEM) [6] and Persson's theory [18, 19]. Further to this binary classification, the comparison between various reported models reveals discrepancies with noticeable differences between each other and with experimental results [17,19–21].

Within the above-mentioned approaches to surface structure simulation, it is also necessary to consider the contact behaviour of an individual asperity ranging from elastic, through elasto-plastic, to fully plastic deformation [8,22–29]. For purely elastic or plastic contact, the classic Hertzian model [30] and fully plastic model [31] can be applied, respectively. However, for elastoplastic regimes, individual asperity models may yield different contact responses, dominated by different deformation mechanisms [32,33]. Particularly, a self-consistent analysis was put forward by Storåkers, et al. [34] considering the general visco-elasto-plastic material indented by a spherical object. Additionally, shoulder-to-shoulder contact models for misaligned asperities were introduced to include oblique contact between pair asperities [15,35,36].

The contact behaviour of individual asperities can be combined to shed light on overall system behaviour by considering statistical and/or fractal approaches to describe surface morphologies. Pioneered by Greenwood and Williamson [7], multi-asperity contact models are based on the statistical height distribution (Gaussian or non-Gaussian), while assuming that the deformation of a given asperity is not influenced by that of neighbouring asperities. Within this framework, various implementations, considering different asperity geometries, have been developed over the past decades for the analysis of individual asperity deformation. In practice, statistical parameters for characterizing surface topography, such as variance of heights, slope, curvature, etc., have been used in this class of contact models. But these implementations assume features at a given narrow range of scales and thus depend on the

* Corresponding author.
E-mail address: yixiang.gan@sydney.edu.au (Y. Gan).

http://dx.doi.org/10.1016/j.ijmecsci.2017.07.018
Received 1 May 2017; Received in revised form 22 June 2017; Accepted 9 July 2017
Available online 10 July 2017
0020-7403/

resolution of the surface measuring apparatus and sample length [13]. However, most natural surfaces exhibit features across a wide range of length scales [37], involving diverse morphologies, which bring about complexities in the modelling of interfacial properties [3,38]. In addition, these statistical models were constructed by assuming that micro-contact forces arise principally due to deformation of asperities and are calculated considering only the base wavelength or a certain range of wavelengths, characterized by the roll-off and cut-off wavevectors of the power spectra of rough surfaces [4,12,17,19,39]. This assumption neglects the contribution of fine geometries at small length scales to the contact properties. In the fractal-theory related models, the finer surface features have been included in terms of overall contact area using an integration process [11,12,28,40].

An early appreciation for the significance of the multi-scale nature of surfaces was demonstrated by Archard [41]. In the contact theory using scale-independent parameters, Majumdar and Bhushan [42] utilized the fractal theory of Mandelbrot [43] to describe the distribution of contact areas between two rough surfaces. Yan and Komvopoulos [12] extended this theory to contact problems of three-dimensional rough surfaces, revealing the variations of the contact force and real contact area during quasi-static loading. Ciavarella, et al. [44] developed a two-dimensional fractal-based model for sinusoidal elastoplastic surfaces, and expanded the analysis to provide contact stiffness and interfacial resistance. Further relevant work was conducted by Jackson and Streator [13] using three-dimensional sinusoidal surfaces, considering the frequency spectrum of the surfaces. Pohrt and Popov [6] deduced an empirical contact stiffness model by means of the boundary element method (BEM). The validity of the method of reduction of dimensionality, by which three-dimensional contact problems are mapped onto one-dimensional elastic contacts, has been investigated for non-adhesive contact of any axisymmetric bodies [45–47]. However, the fractal dimension has been shown to change due to an applied load [38,48,49] and thus an assumption of invariant fractal dimension in fractal-theory related models may only be reasonable within a certain range of loading. Moreover, various methods [20,50,51] can be applied to quantify the fractality of a rough surface [19,20,52,53] possibly resulting in different values of the obtained fractal dimension, thus the adaptation of these methods merits further study to provide a consistent result in contact mechanics models.

The true area of contact formed between two surfaces is of prime interest and is governed by morphology, material properties, and loading conditions. The contact properties of rough surfaces subjected to an applied normal load can be, at some level, interpreted by considering the true interfacial contact area along with surface descriptors [4,46]. However, determining the real contact area between contacting bodies through experimental or numerical analyses remains challenging. Factors that influence true contact area include the asperity height, curvature, the Poisson's ratio of the material, strength and hardness and the existence of superimposed smaller asperities with similar or divergent scale-dependent properties [54]. With time, the sliding induced by expanding contacting spots [55] further affects contact morphology. Moreover, most natural surfaces exhibit features across a wide range of length scales the extent of which depends on simulation or measurement resolution [56,57].

Despite the fact that the contact area tends to present scale-dependent properties with contacting asperities in the status of incomplete contact (with non-contacting zones surrounded by the contacting ones), the truncated areas at various depths for a given resolution can be employed to represent the real contact area. This was first proposed by Abbot and Firestone [31] to describe a wear process rather than indentation or flattening. Along this line, proposed truncation models [58,59] have assumed that the contact area of an asperity pressed against a rigid flat can be approximately calculated by mathematically truncating the asperity tip. This is a reasonable assumption for small to medium interferences as within this range asperities tend to plastically deform due to the small radius of curvature. The average pressure between an asperity and a flat punch can simply be assumed to be equal to hardness, or can be related to material yield strength [7,26]. However, Jackson and Green [22] showed that this simplification results in an inverse hardening process in which the hardness actually decreases with increasing interference.

In addition to contact area the present work focuses on interfacial contact stiffness. An understanding of contact stiffness is important in contact mechanics, which plays a central role in governing the stress-dependent electrical and thermal transport between two contacting solids [6,60,61]. In the past decade, the relationship between surface structure and interfacial stiffness has been intensively studied numerically and experimentally. Numerical analyses, using methods of molecular dynamics, finite element analysis, etc., generally confirm linear proportionality between normal force and contact stiffness [39,62,63], as supported by the Greenwood–Williamson model [7] and Persson's theory [19,64]. However, other studies have reported that, for small to medium loads, the logarithm of stiffness exhibits close proportionality to the logarithm of the applied normal force [6,45,52]. In other words, the contact stiffness, k, is a power function of the normal force, F_N, as $k \propto F_N^{\alpha}$ (with $\alpha < 1$), which differs from the work mentioned above. Numerous experimental studies have been carried out on rough surfaces to ascertain the relationship between surface structure and interfacial behaviour under load using diverse experimental approaches and materials. Jiang, et al. [52] measured the normal contact stiffness of cast iron specimens produced using different machining methods. Wang, et al. [19] measured the contact stiffness of a rubber block squeezed against different concrete and asphalt road surfaces. Buczkowski, et al. [17] compared the normal contact stiffness determined using ultrasonic measurements with the fractal model based on Weierstrass–Mandelbrot function. Zhai, et al. [20] recently evaluated the contact stiffness at aluminium surfaces by nanoindentation tests utilizing different sized flat tips to achieve a wide range of applied stress levels. These experimental studies support the power law relationship between the contact stiffness and the applied load for certain stress ranges.

The main purpose of the paper is to propose a comprehensive contact analysis method for a three-dimensional rough surface compressed by a rigid flat. The proposed truncation method is applied to simulated fractal surface structures characterized using various statistical and fractal descriptors, to interpret the variation of contact stiffness under increasing normal loading using experimental results for reference. Iteration procedures employed in simulating fractal rough surfaces ensure a description with identical parameters which are critical in determining the normal contact stiffness. The applicability and repeatability of the presented method is discussed based on geometrical features and analyses of the studied rough surfaces. This study provides an easily-incorporated and highly-effective numerical method for predicting contact stiffness under conditions of small to medium loads. Following validation, a parametric analysis is conducted for simulated surfaces varying in surface topologies, allowing the obtained contact stiffness to be related to surface roughness descriptors. Finally, correlations between normal contact stiffness and roughness descriptors have been established and discussed with respect to fractal dimension values obtained using different methods.

2. Theoretical framework

The deformation mechanics of contacting surface asperities remains a topic of significant debate in the research community. Under most applied conditions the true contact area between rough surfaces involves only a small fraction of the nominal contact area, and for this reason the total real contact area can be considered to approximately equal to the truncation area in the present method. We consider a simple extension of the contact analysis for indentation by a flat punch [65], which reveals that there is a relation between contact stiffness, contact area, and elastic

modulus, given by

$$E_r(E_c,\ E_i) = \beta\frac{\sqrt{\pi}}{2}\frac{K}{\sqrt{A}}, \tag{1}$$

where K is the contact stiffness in units of N/m, A is the apparent contact area and β is a geometrical constant, taken as unity for a flat punch. E_r denotes the reduced Young's modulus including contributions from the both the compressed rough surface and opposing flat surface, given by $1/E_r = (1-\upsilon_c^2)/E_c + (1-\upsilon_i^2)/E_i$, with the subscript i indicating the opposing surface, the subscript c indicating the properties of the compressed surface and υ being the Poisson's ratio. The contact force can be obtained through integration of the contact stiffness with respect to the indentation increment. Eq. (1) is a fundamental equation for assessing the elastic properties in indentation tests, and has been shown to be equally applicable in cases of elastic-plastic contact. If the elastic modulus is known, the relation between contact area and contact stiffness can thus be obtained [66,67].

2.1. Validation for single asperity under compression

An asperity under compression can behave elastically or plastically. For describing purely elastic contact of rough surfaces, the classic Hertzian model can be applied as suggested by previous contact models [7,26,33,42]. For a sphere under compression by a rigid plane, it is assumed that the radius of a contacting asperity, R, is very close to that of the undeformed case. In such cases, the relationship between R and the truncation microcontact radius, r', can be obtained by $R^2 = (R-d)^2 + (r')^2$, where d is compression depth. Since R is typically orders of magnitude greater than the d, the relationship can be reduced to $(r')^2 = 2Rd$ [12,27]. In Hertzian contact, the radius of the real contact area is given by $r = \sqrt{Rd}$. Thus for a circular microcontact in the fully elastic regime the relationship between the truncation area (a') and the real elastic contact area (a_E) can be expressed as: $a' = 2a_E$.

For describing plastic deformation, Abbot and Firestone [31] developed the most widely used model for a fully plastic contact, known as the surface microgeometry model. This model assumed that the deformation of a rough surface against a rigid flat plane is equivalent to the truncation of the undeformed rough surface at its intersection with the plane. As a result, the real area of the contact can be approximated simply as the geometrical intersection of the flat with the original undeformed surface profile, and the contact pressure is the plastic flow pressure. In addition, McFarlane and Tabor [68] showed that both the normal and tangential stresses contribute to the deformation of junctions formed at the interface of contacting bodies under compression. For cases of elastic contact, the tangential stress constrains the expansion of the compressed asperity through static friction. As the contacting region between an asperity and the rigid flat is already in the plastic state of stress under purely normal loading, tangential loading, however small, may cause further yielding. Equilibrium can be maintained if the area of a contacting spot grows [68]. Therefore, for a fully plastically microcontact, the relation between the truncation area and the real plastic contact area (a_P) is: $a' \le a_P$.

The above discussion supports that the truncation area, a', of a single compressed asperity at any given interference lies in the range of $a_E < a' \le a_P$, the upper and lower limits of which are determined by the contact area for fully elastic and plastic regimes, shown in Fig. 1. For a single asperity of a fractal rough surface, exhibiting a hierarchical structure, we also assume that the contact area of an individual asperity for a given surface interference will follow the relation: $a_E < a' \le a_P$. Furthermore, the truncation method could provide contact properties between elastic and plastic behaviours. This assumption is further rationalized by comparing the dependence of contact area on contact force obtained from the concise self-consistent model for contact of inelastic materials, based on the indentation theory and von Mises isotropic flow theory [9].

For a visco-elasto-plastic contact problem, the constitutive behaviour can be simplified as $\sigma = \sigma_0\varepsilon^{m_B}\dot{\varepsilon}^{n_B}$, where σ_0 is a material yield parameter and m_B and n_B are hardening and creep exponents, respectively. For a time-independent perfectly plastic material, $m_B = n_B = 0$, while in the linearly elastic case, where $m_B = 1$ and $n_B = 0$. A semi-analytical solution for the contact problem can be obtained for spherical bodies [9, 34]. In this paper, only a quasi-static situation is studied without considering creep, i.e., $n_B = 0$. Here, we consider a spherical asperity under compression by a rigid plane using the proposed truncation method and benchmark this special case to other solutions existing in the domain of contact mechanics, in Fig. 2. The maximum interference is 100 times the critical interference, $\omega_c = (\pi kH/2E_r)^2R$ where $k = 0.454 + 0.41\nu$ is the hardness coefficient of the asperity related to its Poisson's ratio, ν, and, H is the hardness of the asperity relative to its yield strength. This critical interference value marks the inception of the elastoplastic deformation [13,26,27]. The elasto-plastic solutions for materials exhibiting different hardening exponents ($m_B = 0.0$, 0.10, 0.20, 0.30, 0.40, 0.50 and 1.0) are shown in Fig. 2. The obtained numerical results from the presented truncation method (1000 truncation depth increments) lie between fully plastic and elastic regimes. Thus, to a certain extent, these results demonstrate the applicability of the truncation method for the analysis of elasto-plastic contact.

2.2. The truncation method for rough surfaces

In this work an approximate model is presented for estimating the contact stiffness of a rough surface compressed by a rigid plane with the following assumptions:

(1) The studied fractal rough surface is flattened by the rigid plane, and contact 'islands' grow in terms of size and number through successive truncations parallel to the mean surface plane;
(2) The truncated surface features on the rough surfaces flow plastically into the valleys of non-contacting regions;
(3) Contacting asperities do not interact with each other;
(4) Deformation is confined within the interface region rather than the bulk region.

In this method, a rough surface is levelled through a mountain-top removal approach in order to obtain truncation areas. For a single asperity under compression, it is a reasonable assumption to use the total truncation area, A' ($A_E < A' = \sum_{i=1}^{i=n} a_i' = A_c < A_F$, where A_c is the true contact area), at a given height to approximate the real contact area for the corresponding surface interference, ω. The contact stiffness is extracted based on the analysis of indentation tests by a flat punch [65]. Under increasing compression, smaller microcontacts expand, merging to form larger ones. Consequently, the value of contact stiffness, E_c depends primarily on the true contact area and approaches the elastic modulus of the bulk material, E. The contact stiffness (k, with the unit of N/m) can be estimated by the following expression using the true contact area (A_c), based on Eq. (1):

$$k = \beta'\frac{2}{\sqrt{\pi}}E_r'\sqrt{A_{c'}} \tag{2}$$

where E_r' is the (constant) reduced elastic modulus calculated for the bulk elastic properties of the tested material (Young's modulus, E and Poisson's ratio, ν) and indenter: $E_r' = [(1-\upsilon^2)/E + (1-\upsilon_i^2)/E_i]^{-1}$, and β' is a geometric factor of the order of unity, equalling to 1. By writing Eq. (2), we assume that the effect of surface roughness on the measured incremental stiffness can be described by considering the true contact area A_c (rather than the projected contact area A) and bulk material properties in Eq. (1). By comparing Eqs. (1) and (2), and considering that $E_i \gg E > E_c$, we obtain the following scaling relation:

$$E_c/E^* \propto \beta'\sqrt{A_c/A}. \tag{3}$$

Considering $\mathrm{d}F = k(\omega)\mathrm{d}\omega$, we can then obtain the loading force F through integration of contact stiffness, $k(\omega)$, during the compression

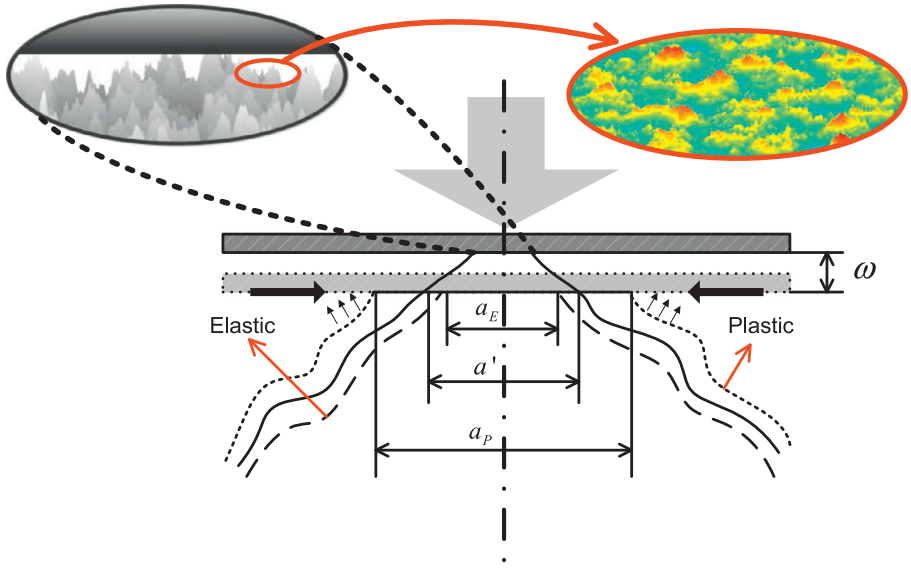

Fig. 1. Schematic of a deformed asperity under compression by a rigid plane. The areas of a_E and a_P, show the real contact areas for fully elastic and plastic regime, respectively, while a' represents the truncation area for a given surface interference of ω.

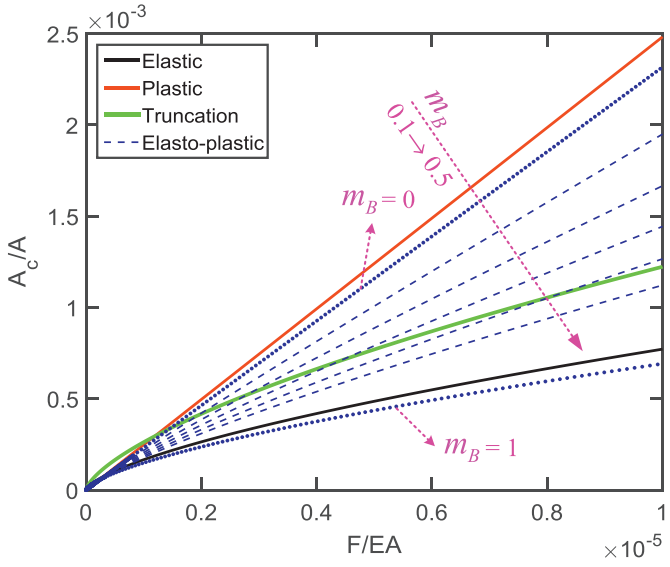

Fig. 2. Comparison of obtained contact responses of a single spherical asperity under compression of a rigid flat between the truncation model and the inelastic flattening model [34]: The normalised contact area versus normalised load is shown with A equalling πR^2, E being the Young's modulus of the material.

with penetration increments dω. Note that we are here focusing on the hierarchical structure of the surfaces by applying normalization procedures.

3. Surface characterization and simulation

To gain insights into the validity of the presently developed truncation method for rough surfaces, we experimentally and numerically evaluated the contact stiffness for round disk samples made of aluminium alloy with surface treatments applied in order to produce distinct surface structures.

3.1. Surface fabrication and profilometry

To produce different rough surfaces, three surface treatment methods were applied: (1) polishing, (2) surface mechanical attrition treatment (SMAT), and (3) abrasive blasting using various sized glass beads. More details of the surface treatment and topographical characterisation can be found in [20]. Fig. 3 shows typical scanning electron microscope (SEM) images, 3D surface topography and corresponding simulated surfaces. Over 10 digitized scans, the treated sample surfaces were characterised through descriptors of the peak-valley height R_t, root mean square roughness R_{rms}, roll-off wavelength W_r, and fractal dimension D characterized through different methods, as shown in Table 1. These roughness descriptors will be used later to generate simulated rough surfaces that have similar features for evaluating the proposed truncation method. Using the fractal dimension we are able to estimate surface structures at scales below the equipment resolution, assuming self-similar scaling in terms of geometrical features [37]. This estimation approach further improves the efficiency of the present method as utilising surface scans at sub-micron scale resolutions, such as those obtained through AFM, would be computationally intensive and would provide limited information from higher scale features.

3.2. Simulated rough surfaces

The scale-invariant parameter, i.e., fractal dimension, provides a means of describing realistic multiscale roughness. Previous studies [12,52,55] have shown that a fractal rough surface can be deterministically simulated by the Weierstrass–Mandelbrot fractal function [43], which can be written as

$$z(x,y) = Wr\left(\frac{G}{W_r}\right)^{(D_{in}-3)}\left(\frac{\ln\gamma}{M}\right)^{1/2}\sum_{m=1}^{M}\sum_{n=0}^{n_{\max}}\left(\gamma^{(D_{in}-3)n}\right) \times\left\{\cos\alpha_{m,n}-\cos\left[\frac{2\pi\gamma^n\left(x^2+y^2\right)^{1/2}}{W_r}\cos\left(\tan^{-1}\left(\frac{y}{x}\right)-\frac{\pi m}{M}\right)+\alpha_{m,n}\right]\right\} \quad (4)$$

The parameter γ determines the density of frequencies used to construct the surface and, in similarity to previous work [33], is set as 1.5 based on considerations of the surface flatness and frequency distribution density. G is a height scaling parameter independent of frequency, termed topothesy [48]. The parameter W_r is the roll-off wavelength, which can be obtained from the power spectrum, determining the basic wavelength of highest scale features. In this paper, values of roll-off wavelength, W_r, of the treated surfaces are obtained by estimating the

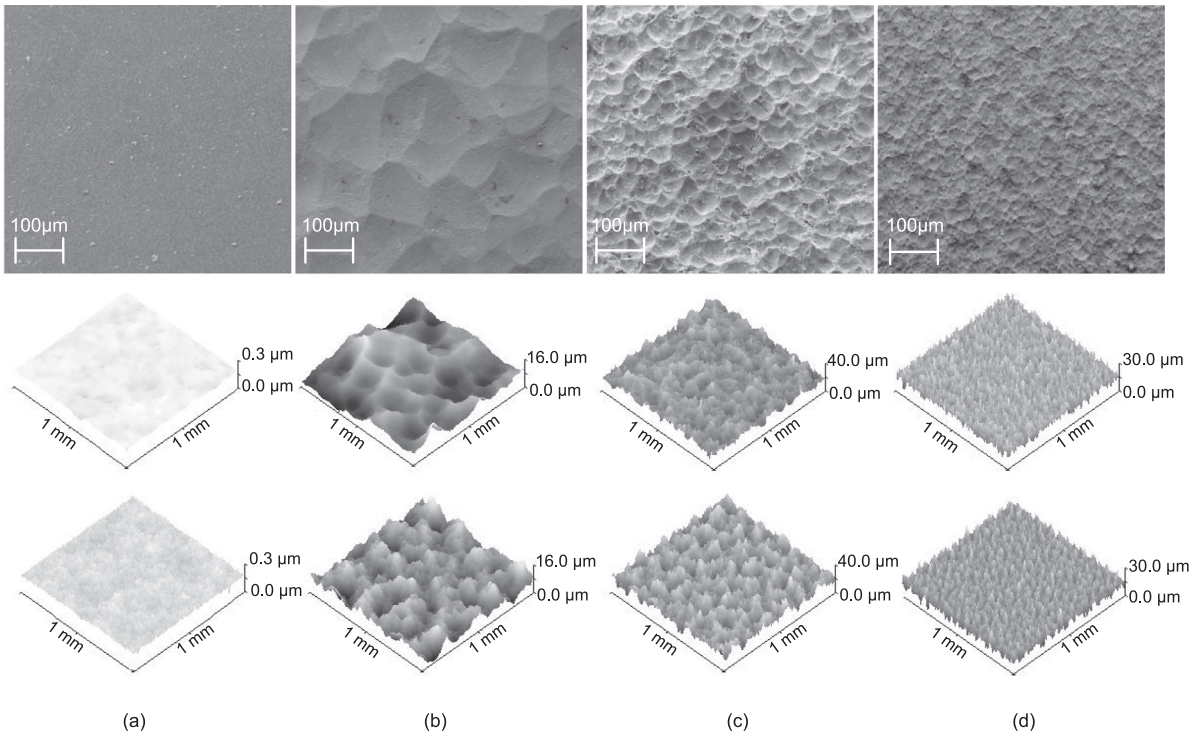

Fig. 3. SEM images, typical digitized profilometry scans (1024 × 1024 pixels over an area of 1 × 1 mm^2) of aluminium samples subjected to different surface treatments and their corresponding simulated surfaces (10, 240 × 10, 240 pixels) presented in row 1, 2 and 3, respectively: (a) polished; (b) SMAT with 2 mm-sized steel balls; (c) blasted with 300 μm-sized glass beads; (c) blasted with 50 μm-sized glass beads.

Table 1
Surface characterisation for digitized scans and simulated surfaces (indicated with a suffix 's' at the end of corresponding sample names).

Surface	Amplitude roughness R_t or R_t' /μm	Root mean square roughness R_{rms} /μm	Roll-off wavelength W_r/μm	Fractal dimension D_{tri}	Fractal dimension D_{box}	Fractal dimension D_{vs}	Fractal dimension D_{sp}
Polished	3.253 ± 1.939	0.057 ± 0.005	≫ 1024	2.093 ± 0.0618	2.024 ± 0.0410	2.103 ± 0.0628	2.317 ± 0.0788
Ps	0.263 ± 0.032	0.053 ± 0.004	≫ 1024	2.091 ± 0.0344	2.025 ± 0.0313	2.103 ± 0.0562	2.315 ± 0.1196
SMAT	22.184 ± 5.201	2.730 ± 0.255	~120	2.228 ± 0.0199	2.156 ± 0.0131	2.422 ± 0.0436	2.412 ± 0.0964
SMATs	16.210 ± 1.569	2.762 ± 0.053	120	2.225 ± 0.0232	2.161 ± 0.0297	2.417 ± 0.0487	2.421 ± 0.1222
GB300	42.376 ± 9.238	4.179 ± 0.194	~60	2.551 ± 0.0217	2.424 ± 0.0257	2.811 ± 0.0769	2.284 ± 0.0931
GB300s	36.865 ± 1.731	4.102 ± 0.034	60	2.555 ± 0.0425	2.417 ± 0.0316	2.813 ± 0.0521	2.282 ± 0.0876
GB50	32.239 ± 7.843	2.970 ± 0.276	~25	2.626 ± 0.0174	2.351 ± 0.0363	2.824 ± 0.0767	2.279 ± 0.1054
GB50s	26.239 ± 1.157	2.935 ± 0.031	25	2.625 ± 0.0328	2.351 ± 0.0395	2.825 ± 0.0876	2.284 ± 0.0933

average distances between asperities, based on surface structures measured experimentally. The frequency index n_{max} assumes finite values corresponding to the cut-off wavelength, W_c, representing the smallest distance between two adjacent pixels [12,55]. The parameter M denotes the number of superposed ridges used to construct the surface. A random number generator is used to uniformly distribute the values of random phase $\alpha_{m,n}$. Here, isotropic fractal surfaces, consisting of 10,240 × 10,240 pixels, with $M = 10$, were generated to simulate real surfaces based on the surface descriptors obtained from digitized scans with the projective area being 1 mm × 1 mm, shown in Fig. 3.

In the fractal analysis of surface asperities, the fractal dimension and the topothesy as are commonly considered as two invariants. However, these two roughness parameters have been shown to vary with load [48]. In this paper, a scaling procedure based on amplitude roughness, R_t, was employed to govern the vertical properties of simulated surfaces instead of topothesy, G (set as 1). The values of all pixels, representing the height, were scaled according to the height-width ratio (R_t/L, where L is the side length of the surface) of the simulated surface, in order to yield the target peak-valley height. The fractal dimension of rough surfaces (for both digitized scans and simulated surfaces) was then estimated using methods of (1) triangulation [20,69], (2) box-counting [70,71], (3) vertical sections [51], and (4) power spectrum analysis (Mitchell and Bonnell, 1990; Williams and Beebe Jr, 1993; Van Put et al., 1994; Mannelquist et al., 1998), with the obtained fractal dimension marked with D_{tri}, D_{box}, D_{vs}, and D_{sp}, respectively. The four methods employed are widely used in the calculation of fractal dimension [61,72–74], though the resulting fractal dimension may be not identical. As is shown schematically in Fig. 4, the procedure for obtaining the input fractal dimension D_{in} for simulated surfaces involves assuming an initial value of D_{in} (e.g., the value obtained from the real surface scan). A surface (1024 × 1024 pixels over an area of 1 × 1 mm^2) is generated with inputting other required parameters, i.e., the roll-off wavelength W_r and amplitude roughness R_t. Subsequently, the calculated value of fractal dimension, D_{out}, of the generated surface is compared with the value obtained from the real surface scan and D_{in}, is adjusted accordingly. This procedure is repeated until the calculated fractal dimension, D_{out}, approaches that determined from the profilimetry of real surfaces using one chosen method (e.g., error < 5%). Even though the triangulation, box-counting method, vertical sections approaches and power spectrum analysis result in different values of fractal dimension, a larger input fractal dimension consistently leads to a larger evaluated D_{out}, with all four approaches.

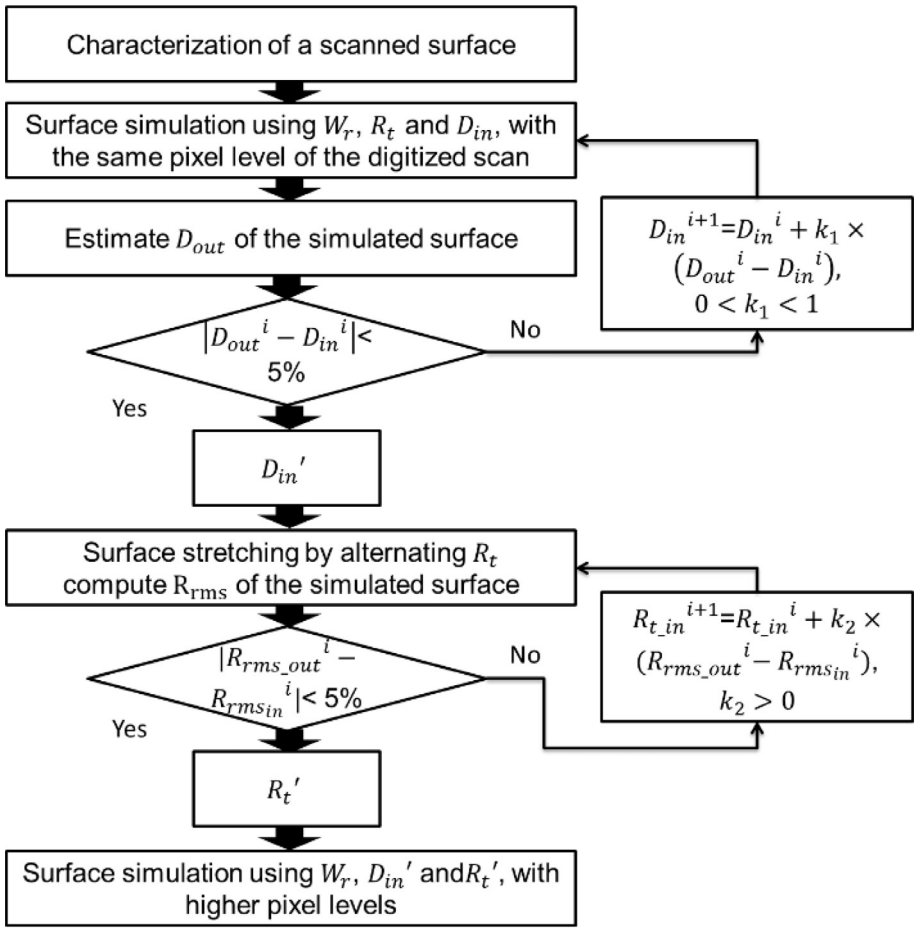

Fig. 4. Flow chart of iterative procedures for surface simulation.

As amplitude roughness R_t from digitized scans is sensitive to measurement resolution and noise, R_{rms} is employed to yield vertical features approximating real surfaces. Similar to the fractal dimension, an iteration procedure is employed to obtain a proper R_t' value with which a simulated surface can replicate the vertical geometrical features of the digitized scans. Subsequently, the obtained D_{in}' and R_t' from the iteration procedures, along with the basic wavelength, W_r, are used to generate rough surfaces at higher resolutions. The sequence of the two iteration procedures, for D_{in}' and R_t' should not be reversed, as the variation of input fractal dimension can influence the roughness amplitude, but not vice versa. The simulation of surfaces using the proposed iteration procedures are presented in Fig. 4.

The amplitude roughness, R_t, and the RMS roughness, R_{rms}, have been shown to be scale-dependent, which can be determined by the roll-off and cut-off wavelength [11]. The values of the two parameters used in the iteration procedure, shown in Fig. 4 and Table 1, are those calculated at the scanning resolution.

3.3. Influences of resolution

As the true contact area between real surfaces is difficult to definitively determine, it is important to investigate the influences of the surface resolution, as well as step sizes of truncating increments. The total contact area can be determined by summarising the contribution of contacting asperities. For a given truncation, the total truncated area, is decreasing as the resolution increases [12,43].

The contact stiffness obtained using the proposed method was studied using simulated surfaces of varied resolution. Results obtained from scans with resolution ranging from 1024×1024 to $32{,}760\times32{,}760$ pixels over an area of $1\times1\,mm^2$ are compared in Fig. 5(a). The effects of truncation increment size are shown in Fig. 5(b). For both scenarios, the maximum truncation depths are up to half of the roughness amplitude, which is roughly the mean plane of the rough surface. The shaded error bars are obtained from ten simulations for each resolution and truncation step size. For relatively low-resolution surfaces, a clear resolution-dependence can be observed, while this trend tends to diminish as resolution increases. Similarly, simulations using 200 or more increments, up to 5000, appear to have small differences. Therefore, a resolution higher than 8192 × 8192 with more than 200 increment steps appears sufficient for the truncation method to provide results yielding negligible resolution sensitivity and numerical convergence.

With an increasing resolution, the contact area, and therefore, the contact stiffness approaches the asymptotic limit. This is consistent with the other fractal-based models [3,4,13,14,18], in which scale-independent contact area and contact stiffness can be achieved. Even though a converging trend has been observed based on the proposed framework, the question remains on quantitatively estimating the contact area, interfacial void, contact resistance, and any other quantity which depends on extremely fine details. The ongoing fractality shown by the hierarchical surface structures may effectively become less important for interfacial properties on a critical length scale marking the defined mechanical interaction, electron transport, heat transfer, etc. This can be generally supported by experimental research with observed values of interfacial parameters, such as contact stiffness, electrical contact resistance, and friction etc. [3,20,52,61,62,75–77]. This convergence trend will be discussed in details in our following work. In this paper, the horizontal resolution of the generated surface is set as around 100 nm, i.e., $10{,}240\times10{,}240$ pixels over an area of $1\times1\,mm^2$, and 200 incre-

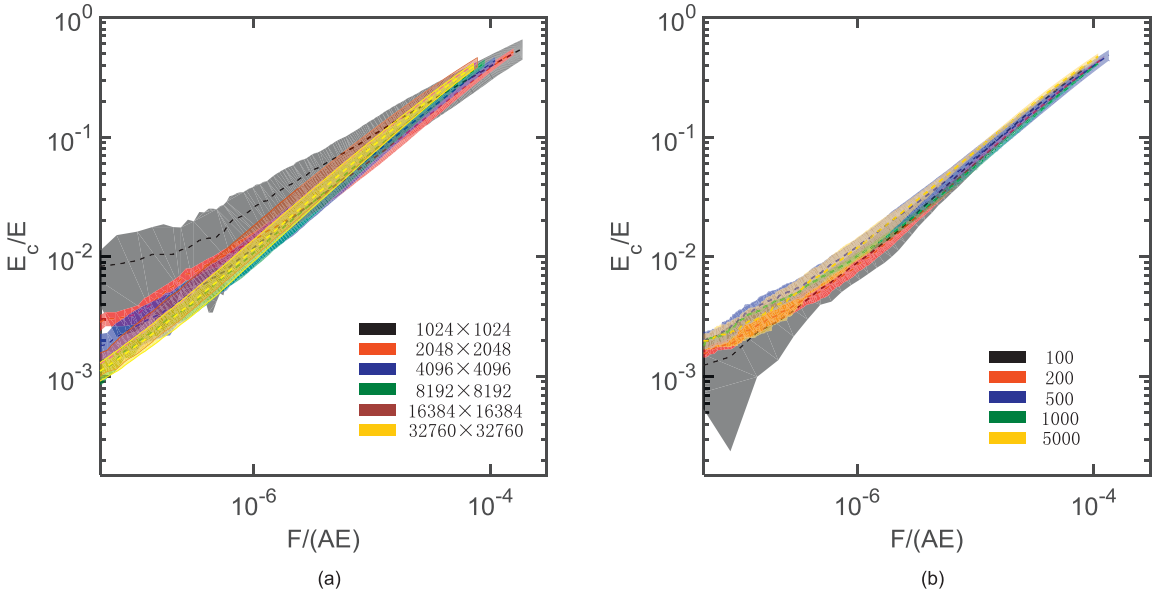

Fig. 5. Sensitivity studies on spatial resolution and increment steps on the calculated contact stiffness using the truncation method: (a) pixel level; (b) number of increment steps. The inputs of the compressed surfaces are as follows: $D_{in}=2.5$, $R_t=10{,}000$ nm and $W_r=100$ μm.

ment steps are considered in the integration process for estimating the contact force.

4. Applications and discussion

4.1. Nanoindentation on roughened surfaces

The normal contact stiffness of three types of treated surfaces was assessed using nanoindentation (Agilent G200) with three flat indenter tips of different diameters of 54.1 μm, 108.7 μm and 502.6 μm (FLT-D050, FLT-D100, and FLT-D500, respectively, SYNTON-MDP). In order to evaluate only the elastic responses, partial unloading tests were successively performed at ten intervals by decreasing the applied load by 10% each time. The loading level of each successive unloading stage is twice that of the preceding one, with a maximum load of 500 mN reached during the final unloading step [20,61]. The obtained contact stiffness, in units of N/m was further transformed to surface stiffness in units of Pa through $E_C=(\sqrt{\pi}K)/(2\sqrt{A})$ where A is the projected area of the flat indentation tip. The experimental results show that the relation between the contact modulus and applied loading force can be described as $E_c/E=\beta[F/(EA)]^{\alpha}$. Correlations between the surface parameters and, α and β the evaluated are detailed in [20]. From the present experiments, the exponent α of the obtained power law relation shows strong dependence on surface fractality, while the roughness amplitude is found to govern the magnitude of parameter β. The maximal indentation depth reached is around 5 μm, which is comparable with the roughness amplitude. The experimentally observed low-level compression depths suggest that the contact stiffness over a wide stress range is strongly affected by finer surface details, which are superimposed on the basic waves. These finer features may not be included in the study of contact mechanics governed by the surface structure [3–5,12]. Specifically, the considered finest feature of the roughness can be different in various engineering applications. The electrical contact resistance [61,76] and adhesion [78] have found to be sensitive to fine surface structures at smaller length scales. However, the influences of surface structures on interfacial thermal conduction can be well described using RMS surface roughness, which depends primarily on basic wavelength [79].

4.2. Comparison with experimentally measured contact stiffness

Contact analyses using the proposed truncation method are presented in Fig. 6. For SMAT and GB surfaces, the numerical results obtained from simulated surfaces are in good agreement with experimental results, particularly for low applied pressures, corresponding to small truncation depths, in the range 0 to 10.0 ~ 15.0% R_t', 30.0 ~ 35.0% R_t', 32.5 ~ 37.5% R_t', and 25.0 ~ 30.0% R_t' for simulated surfaces, Ps, SMATs, GB300s, and GB50s, respectively.

It can be found in Fig. 6 that the predicted results for polished samples show the most significant divergence between numerical and experimental results in particular for interferences greater than 15% R_t'. This is likely the result of several factors, notably the misalignment of the indenter with tested surfaces and roughness features that may be present on the flat diamond tip (measured to have an RMS roughness of around 0.05 μm) as well as adhesion, boundary effects and surface hydration, all of which yield a more pronounced effect for polished surfaces. Even though differences between the numerical analyses and experimental results can be noticed, by comparing the numerical results obtained from the mentioned models with the experimental results, we can systematically deduce the following conclusions: (1) power-law relation between the contact stiffness of a fractal rough surface and the normal load is found; (2) the roughness amplitude represented by R_t and R_{rms} plays a considerable role in determining the amplitude of the function; (3) the slope of the obtained power functions of the contact stiffness on applied normal force are in the range [1/3, 1), depending mainly on the fractal property of the surface. Comparative analyses of the experimental results with existing models can be found in [16,17,20,52,61]. It worth noting that linear relationship can be obtained within a certain range of normal compression, as shown in [17,19,64,80]. More importantly, in this paper, power-law relationships over a wide range of normal compression load have been experimentally observed and numerically demonstrated using our proposed method, covering the small-to-medium load.

4.3. Applicable truncation depth

As shown in the previous section, the proposed truncation method is capable of efficiently extracting contact stiffness on the basis of surface

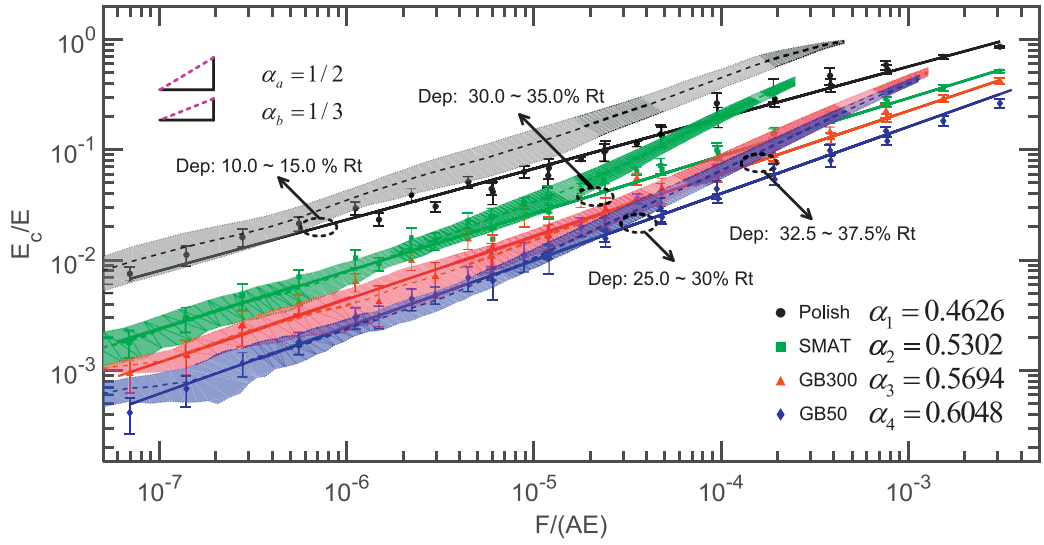

Fig. 6. Comparison of the experimental results and the contact stiffness obtained using the truncation method using D_{vs} . Normalised stiffness, E_C/E, and normalised applied load, $F/(EA)$, are used, with E being the Young's modulus of the tested material, and A the apparent contact area. The numerical results based on the present method are shown using dashed lines with shaded error bars. Solid lines (representing the fitted power functions with the exponent values provided) with error bars are for experimental results.

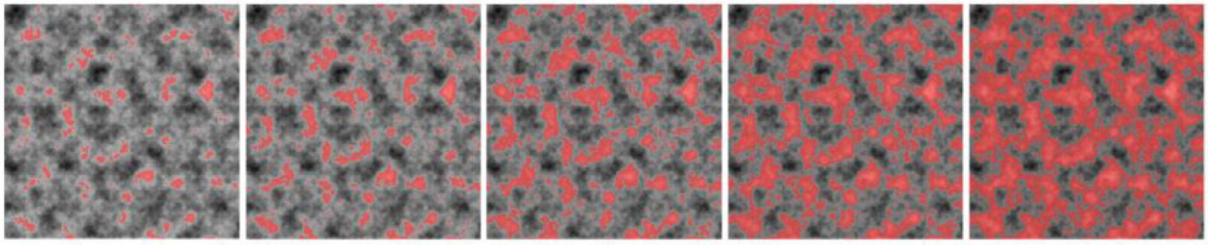

Fig. 7. Truncation sections for a typical scanned GB surface at varying heights. The truncation starts from the top of the surface with depths of 10%R_t, 20%R_t, 30%R_t, 40%R_t, and 50%R_t, and the estimated contact areas are coloured with red.

descriptors for small to medium loads. This method provides an easily implemented numerical framework to relate contact behaviour to the geometrical description of studied surfaces, with tunable resolution and calculation accuracy, meeting the requirements for various engineering applications. However, as the load and the truncation depth increase, the applicability of the presented method merits further discussion, due to the complex deformation of the compressed asperities, interaction between neighbouring asperities, adhesion, and friction. The applicable interference range is discussed below by concentrating on the surface geometries and asperity interactions.

In this model, for a given surface interference, the total contact area under compression is simply determined from numerical integration of the truncated areas of the rough surfaces, at the corresponding truncation height. As shown in Fig. 6, the proposed numerical procedure is capable of predicting the contact stiffness until the truncation depth reaches a certain value. A series of truncation sections for a typical GB300s surface are shown in Fig. 7. As the surface interference increases, small contacting spots expand, giving rise to increased interactions between asperity contact regions. A uniform rise in the height of the non-contacting regions has been experimentally observed [81], showing interactions also at asperity bases. Increasing compression can also bring about a variation in asperity shape. As the surfaces approach, contacting spots continue to grow and merge with each other, with mechanical behaviour transitioning gradually to that of a bulk material. These phenomena at large surface interferences result in limitations to the present truncation method beyond a certain level of deformation.

In order to quantitatively define the applicable range of the truncation method, we firstly consider the variation of island numbers with respect to depth, which can be employed to indicate the interaction between asperities. The numbers of contacting asperities at various truncation depths for the four types of studied surfaces over a projected area of $3\times3\,\mathrm{mm}^2$ with $30{,}720\times30{,}720$ pixels are shown in Fig. 8(a). This size is chosen to give a meaningful statistical representation of the islands. As the interference depth increases, the number of contacting spots reaches a maximum at depths larger than those maximum truncation depths. The range of truncation depths in which the growth rate of island numbers increases monotonically coincides with the applicable range of the present method, as shown in Table 2. Furthermore, we considered the evaluation of perimeters and areas of all levelled islands at varying truncating heights using the approach proposed by Mandelbrot (1984). The correlation law between perimeter, L_T, and Area, A, for sections of truncated asperities, like islands surrounding by water, is given by:

$$L_T \propto A_T^{(D_{vs}-1)/2}. \tag{5}$$

Within a certain range, the correlation between perimeter and area follow a power law type behaviour for all the four types of studied surfaces. However, as the truncation depth further increases, the exponent experiences a downward trend as is shown in Fig. 8(b), departing from the power law behaviour shown in Eq. (5). This suggests a critical truncation depth range, in which a truncated surface can be described by an invariant fractal dimension. In this paper, at any given truncation depth, the curve fitting between L_T and A are conducted, with all obtained data for L_T and A to extract the exponent value, and the critical depth is obtained as an obvious decrease for the exponents is observed, as listed in Table 2. The exponents of the obtained power law relations are all larger than 0.5, which is the typical value of the exponent obtained in verti-

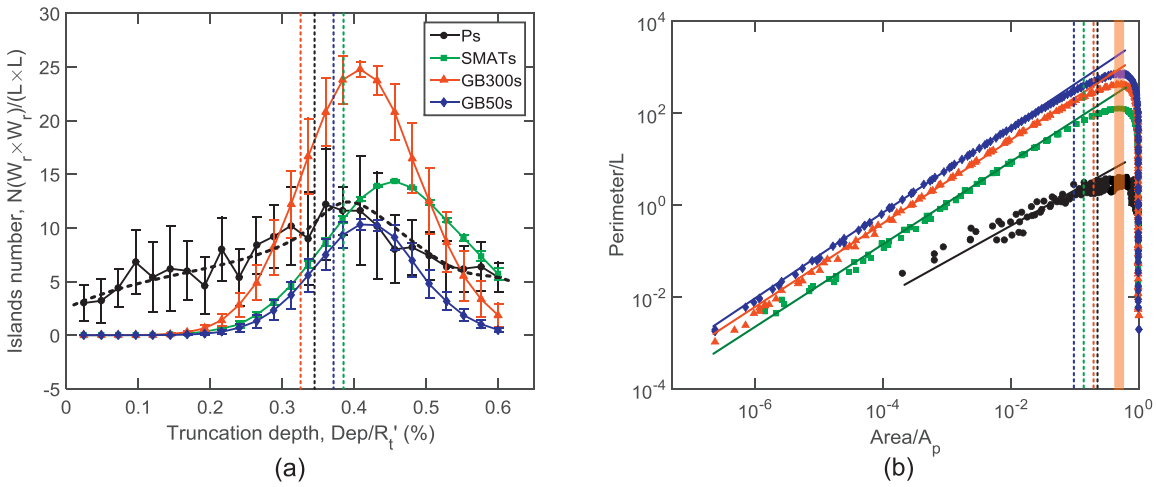

Fig. 8. Surface geometry analyses: (a) normalised numbers of contacting spots at various truncation depths for the studied surfaces, where the critical truncation depths, corresponding to maximal growth rates of island numbers, are marked with dashed lines; (b) typical log-log plots based on slit island analysis for the four types of studied surfaces (four simulations have been carried out for each type of surfaces) with the solid lines having a respective the exponent value, shown in Eq. (5).

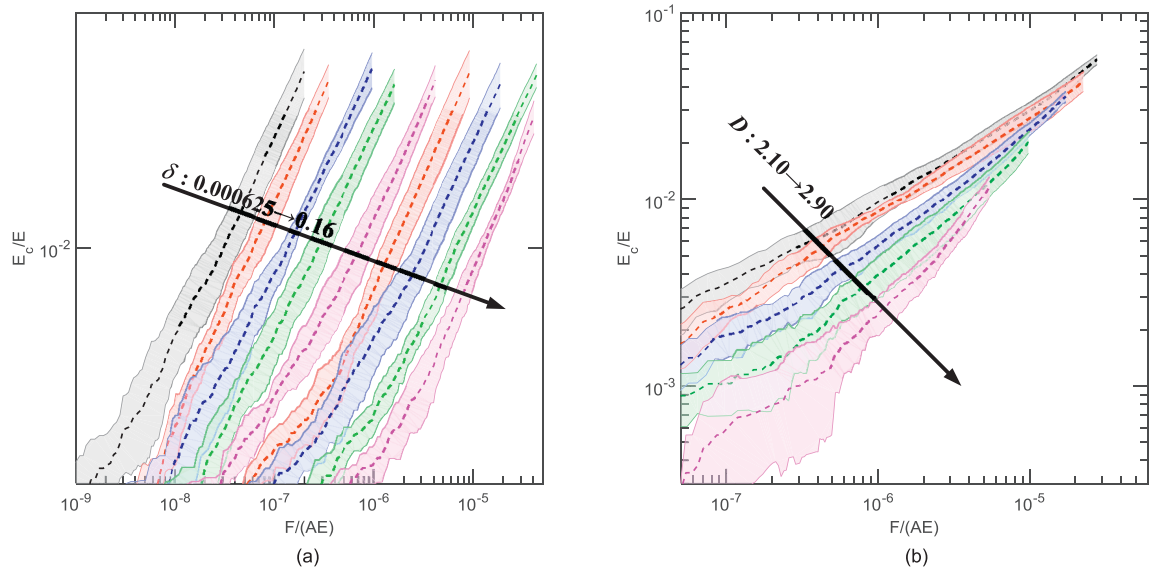

Fig. 9. Dependence of the normal contact stiffness on the normal pressure: (a) for constant fractal dimension, $D_{in} = 2.5$ and different relative roughness δ; (b) constant relative roughness $\delta = 0.01$ and different fractal dimension D_{in};.

Table 2
Indicators for the applicable range of the proposed truncation method.

Surface	Maximum applicable depth for truncation method (% R_t)	Depth for the maximum increasing rate of island number (% R_t)	Maximum depth for surface exhbiting fractality (% R_t)
Ps	10.0–15.0	33.0–33.5	25.0–30.0
SMATs	30.0 –35.0	36.0–36.5	32.5–37.5
GB300s	32.5–37.5	31.0–31.5	30.0–35.0
GB50s	25.0–30.0	34.0–34.5	27.5–32.5

cal section analysis for an asperity in regular shape, such as a sphere or cone.

Despite the fact that the two indicators we choose here are based only on surface topology, these geometrical features are closely related to the mechanical responses under normal compression. Within the range of truncation depths suggested by the two indicators, contacting asperities tend to be sufficiently isolated and thus respond to the external loading individually. Moreover, in this range, an invariant fractal dimension can be applicable to describe the multi-scale nature of the surface. At a truncation depth beyond this range, interactions between neighbouring asperities will have a significant influence on the contact, causing a change of asperity shape, non-ignorable adhesion, sliding at interfaces etc. Even though the applicable range may also be affected by the mechanical properties of the material, including hardening, Poisson's ratio, and scale-dependent yielding strength, the purpose of this paper is to present a numerical framework to consider the structure dependent contact behaviour.

4.4. Parametric study using the truncation method

In order to relate the surface structure, represented by descriptors including fractal dimension, roughness amplitude and wavelength, to

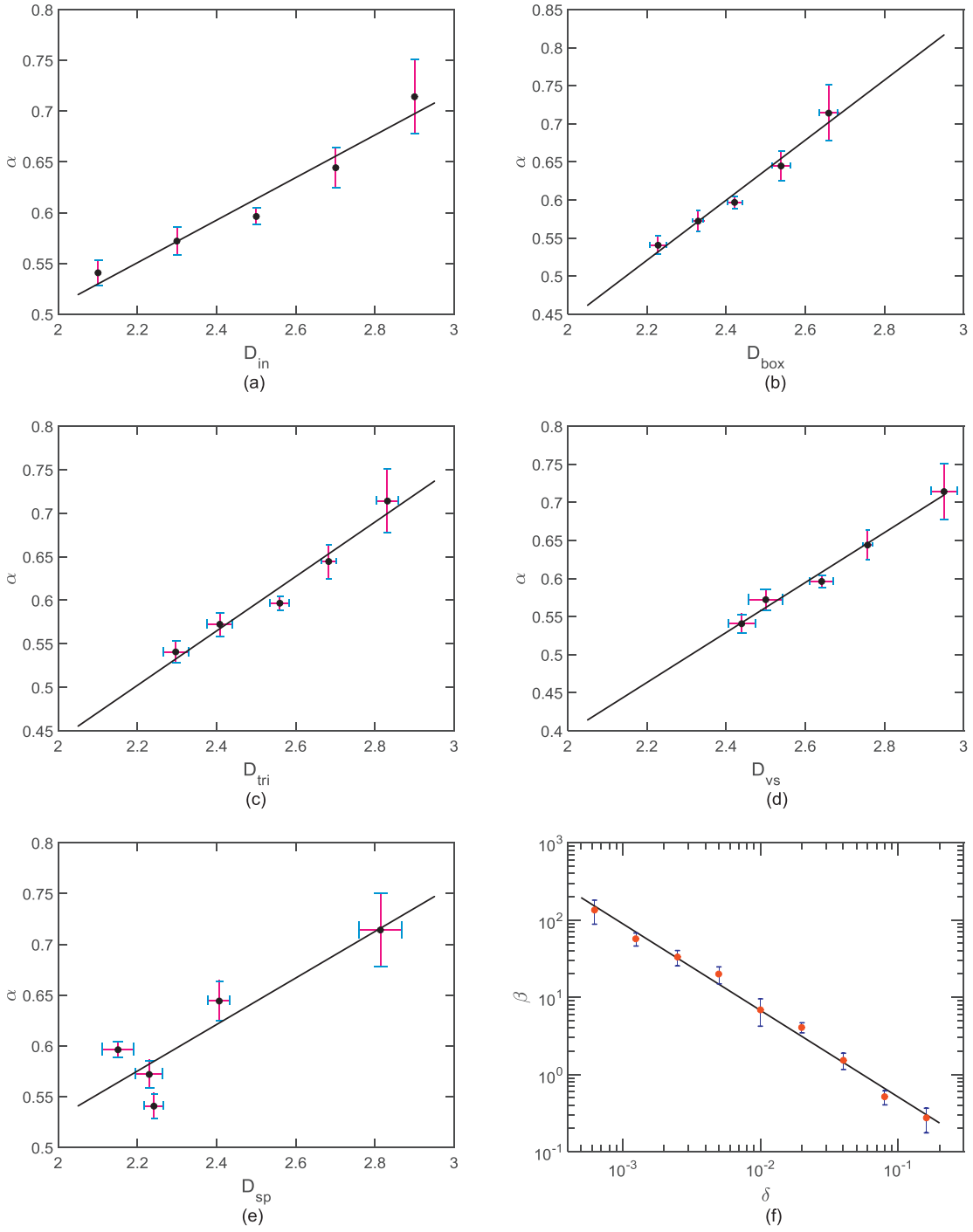

Fig. 10. (a–e) Correlation between the stiffness variation exponent α and values of fractal dimension characterized using different methods; (f) Correlation between the stiffness magnitude β and values of roughness amplitude, δ. Horizontal and vertical error bars show the corresponding standard deviations from the surface measurement and curve fitting.

contact stiffness, contact analyses are conducted for fractal rough surfaces with various surface topographies. The contact analyses were performed under conditions of small surface interferences as discussed in the previous section, in a regime where the truncation method performs well. Two groups of surfaces (10,240×10,240 pixels over an area of $1\times1\,mm^2$) were generated and analysed by the present model, with the maximum surface interference being $0.1R_t$. One group of simulated surfaces was generated with a constant fractal dimension value of $D_{in}=2.50$ and a varied roughness amplitude δ (0.000625, 0.00125, 0.0025, 0.005, 0.01, 0.02, 0.04, 0.08, and 0.16). For the second group, surfaces were set with the same relative roughness amplitude, described as $\delta=R_t/W_r=0.01$ and exhibited varying fractality D_{in} (2.10, 2.30, 2.50, 2.70, and 2.90). In order to further test the repeatability of the present model, we analysed five simulated surfaces for each individual set of input roughness parameters. Fig. 9 shows that the predicted contact stiffness exhibits a power-law relation with the applied normal load, which can be described as $E_c/E=\beta[F/(EA)]^{\alpha}$. The parameters of exponent α and magnitude β are related only to surface structure. The exponent α increases with values of fractal dimension, D_{in}, while the relative roughness amplitude, δ, indicating primarily the vertical scale of the rough surface, dominates β. The correlations for the stiffness parameters, i.e.,

Table 3
Fitting functions for the stiffness parameters, α and β, using D_{in} and δ.

Fractal dimension	α	Coefficient of correlation (for α)	β	Coefficient of correlation (for β)
D_{in}	$\alpha = 0.209D_{in} + 0.090$	0.940	\	
D_{tri}	$\alpha = 0.313D_{tri} - 0.186$	0.948	\	
D_{box}	$\alpha = 0.394D_{box} - 0.347$	0.966	\	
D_{vs}	$\alpha = 0.328D_{vs} - 0.258$	0.980	\	
D_{sp}	$\alpha = 0.229D_{sp} + 0.071$	0.741	\	
δ	\		$\beta = 0.0386\ \delta^{-1.122}$	0.992

α and β, using δ and D were obtained and shown in Fig. 10. The corresponding fitted functions are presented in Table 3.

The plots shown in Fig. 10 examine the effects of using different methods for the evaluation of the fractal dimension of rough surfaces in contact [3,6,11–13,20,61], namely the triangulation method (D_{tri}), box-counting method (D_{box}), vertical sections method (D_{vs}), and power spectrum analysis (D_{sp}). The obtained fractal dimensions are expected to differ somewhat due to the use of different calculation methods. As shown in Fig. 10 and Table 3, using fractal dimension obtained from different methods will produce different fitting functions in terms of $\alpha(D)$. Thus it is necessary to clarify how the fractal dimension is extracted and the applicable interference and/or load range of the chosen approach of contact mechanics. However, the regression factors for fitting functions, $\alpha(D)$, are greater than 0.94 in most cases, except the one using the power spectrum analysis, demonstrating a strong correlation with fractality.

5. Conclusion

In this paper, we propose an efficient numerical approach for calculating the contact stiffness of fractal rough surfaces under compression by considering a series of truncation sections and discuss the applicable range of this method. Numerical predictions of contact stiffness are benchmarked with experimental data over a wide range of applied normal loads, showing a quantitative agreement with measurements for a range of different rough surfaces. Parametric analyses were carried out for simulated surfaces with varying surface topologies, to establish correlations between the obtained contact stiffness and surface roughness descriptors, including the fractal dimension and roughness amplitude. Based on the results and discussion presented, the following conclusions can be drawn:

(1) Fractal rough surfaces can be well described using three key parameters including roll-off wavelength, amplitude roughness and fractal dimension. For diverse surface structures flattened by a rigid flat, a unified power law function between the contact stiffness and the contact load can be found both experimentally and numerically. The exponent of the obtained power law relation increases with values of fractal dimension, while the magnitude decreasing exponentially with the relative roughness amplitude.
(2) The numerical solutions of the proposed method for contact stiffness versus contact load are in good agreement with experimental results over a wide range of normal compression. The surface interference range over which the proposed truncation method is applicable, can be determined by monitoring the variation of the number of contact islands in truncated sections, and the evolution of the total perimeter and area of these islands, as truncation deepens. These geometrical features are closely related to the mechanical responses under normal compression indicating the interactions between asperities. Within the applicable range, an invariant fractal dimension can be employed to present the hierarchical properties of the surface structure.
(3) The parametric analyses presented in this study suggest that different methods for characterizing the fractal dimension of a rough surface may lead to different predicted contact stiffness within the applicable interference for approaches based on fractal theory. This implies that the characterization method applied to determine this surface descriptor can affect somewhat the predicted contact mechanics.

Acknowledgements

Financial support for this research from the Australian Research Council through grants DE130101639 is greatly appreciated. C.Z. acknowledges the financial support from Endeavour Prime Minister's Australia Asia Scholarship for conducting his PhD research project at The University of Sydney.

References

[1] Popov VL. Contact mechanics and friction. Berlin: Springer Science & Business Media; 2010.
[2] Persson BNJ. Contact mechanics for randomly rough surfaces. Surf Sci Rep 2006;61:201–27.
[3] Persson B, Albohr O, Tartaglino U, Volokitin A, Tosatti E. On the nature of surface roughness with application to contact mechanics, sealing, rubber friction and adhesion. J Phys 2005;17:R1.
[4] Carbone G, Bottiglione F. Asperity contact theories: Do they predict linearity between contact area and load? J Mech Phys Solids 2008;56:2555–72.
[5] Carbone G, Bottiglione F. Contact mechanics of rough surfaces: a comparison between theories. Meccanica 2011;46:557–65.
[6] Pohrt R, Popov VL. Normal contact stiffness of elastic solids with fractal rough surfaces. Phys Rev Lett 2012;108:104301.
[7] Greenwood J, Williamson J. Contact of nominally flat surfaces. In: Proceedings of the royal society of London. Series A. Mathematical and physical sciences, 295; 1966. p. 300–19.
[8] Bush A, Gibson R, Thomas T. The elastic contact of a rough surface. Wear 1975;35:87–111.
[9] Larsson J, Biwa S, Storåkers B. Inelastic flattening of rough surfaces. Mech Mater 1999;31:29–41.
[10] Kogut L, Etsion I. A static friction model for elastic-plastic contacting rough surfaces. J Tribol 2004;126:34–40.
[11] Majumdar A, Tien C. Fractal characterization and simulation of rough surfaces. Wear 1990;136:313–27.
[12] Yan W, Komvopoulos K. Contact analysis of elastic-plastic fractal surfaces. J Appl Phys 1998;84:3617–24.
[13] Jackson RL, Streator JL. A multi-scale model for contact between rough surfaces. Wear 2006;261:1337–47.
[14] Ciavarella M, Dibello S, Demelio G. Conductance of rough random profiles. Int J Solids Struct 2008;45:879–93.
[15] Hanaor DA, Gan Y, Einav I. Contact mechanics of fractal surfaces by spline assisted discretisation. Int J Solids Struct 2015;59:121–31.
[16] Chen Q, Xu F, Liu P, Fan H. Research on fractal model of normal contact stiffness between two spheroidal joint surfaces considering friction factor. Tribol Int 2016;97:253–64.
[17] Buczkowski R, Kleiber M, Starzynski G. Normal contact stiffness of fractal rough surfaces. Archiv Mech 2014;66:411–28.
[18] Persson B. Elastoplastic contact between randomly rough surfaces. Phys Rev Lett 2001;87:116101.
[19] Wang D, Ueckermann A, Schacht A, Oeser M, Steinauer B, Persson B. Tire–road contact stiffness. Tribol Lett 2014;56:397–402.
[20] Zhai C, Gan Y, Hanaor D, Proust G, Retraint D. The role of surface structure in normal contact stiffness. Exp Mech 2016;56:359–68.
[21] Raffa ML, Lebon F, Vairo G. Normal and tangential stiffnesses of rough surfaces in contact via an imperfect interface model. Int J Solids Struct 2016;87:245–53.
[22] Jackson RL, Green I. A finite element study of elasto-plastic hemispherical contact against a rigid flat. J Tribol 2005;127:343–54.
[23] Brake M. An analytical elastic-perfectly plastic contact model. Int J Solids Struct 2012;49:3129–41.
[24] Shankar S, Mayuram M. Effect of strain hardening in elastic–plastic transition behavior in a hemisphere in contact with a rigid flat. Int J Solids Struct 2008;45:3009–20.
[25] Greenwood J. A simplified elliptic model of rough surface contact. Wear 2006;261:191–200.
[26] Chang W, Etsion I, Bogy DB. An elastic-plastic model for the contact of rough surfaces. J Tribol 1987;109:257–63.

[27] Kogut L, Etsion I. Elastic-plastic contact analysis of a sphere and a rigid flat. J Appl Mech 2002;69:657–62.
[28] Jackson RL. An analytical solution to an Archard-type fractal rough surface contact model. Tribol Trans 2010;53:543–53.
[29] Kogut L, Komvopoulos K. Analysis of the spherical indentation cycle for elastic–perfectly plastic solids. J Mater Res 2004;19:3641–53.
[30] Hertz H. On the contact of elastic solids. J Reine Angew Math 1881;92:156–71.
[31] Abbot E, Firestone F. Specifying surface quality. Mech Eng 1933;55:569–72.
[32] Mesarovic SD, Fleck NA. Spherical indentation of elastic–plastic solids. In: Proceedings of the royal society of London A: mathematical, physical and engineering sciences. The Royal Society; 1999. p. 2707–28.
[33] Kogut L, Jackson RL. A comparison of contact modeling utilizing statistical and fractal approaches. J Tribol 2006;128:213–17.
[34] Storåkers B, Biwa S, Larsson P-L. Similarity analysis of inelastic contact. Int J Solids Struct 1997;34:3061–83.
[35] Li B, Hong J, Shao G, Du F. An integrated mechanical–electrical predictive model of electrical contact resistance between two rough surfaces. Tribol Trans 2015;58:537–48.
[36] Sepehri A, Farhang K. On elastic interaction of nominally flat rough surfaces. J Tribol 2008;130:011014.
[37] Persson B. On the fractal dimension of rough surfaces. Tribol Lett 2014;54:99–106.
[38] Hanaor D, Einav I, Gan Y. Effects of surface structure deformation on static friction at fractal interfaces. Géotech Lett 2013;3:52–8.
[39] Campana C, Persson B, Müser M. Transverse and normal interfacial stiffness of solids with randomly rough surfaces. J Phys 2011;23:085001.
[40] Chung JC, Lin JF. Fractal model developed for elliptic elastic-plastic asperity microcontacts of rough surfaces. J Tribol 2004;126:646–54.
[41] Archard J. Elastic deformation and the laws of friction. In: Proceedings of the royal society of London. Series A. Mathematical and physical sciences, 243; 1957. p. 190–205.
[42] Majumdar A, Bhushan B. Role of fractal geometry in roughness characterization and contact mechanics of surfaces. J Tribol 1990;112:205–16.
[43] Mandelbrot BB. The fractal geometry of nature. Macmillan; 1983.
[44] Ciavarella M, Murolo G, Demelio G. The electrical/thermal conductance of rough surfaces—-the Weierstrass–Archard multiscale model. Int J Solids Struct 2004;41:4107–20.
[45] Pohrt R, Popov VL. Contact stiffness of randomly rough surfaces. Sci Rep 2013;3:3293.
[46] Pohrt R, Popov VL, Filippov AE. Normal contact stiffness of elastic solids with fractal rough surfaces for one-and three-dimensional systems. Phys Rev E 2012;86:026710.
[47] Popov VL. Method of reduction of dimensionality in contact and friction mechanics: a linkage between micro and macro scales. Friction 2013;1:41–62.
[48] Liou JL, Lin JF. A new method developed for fractal dimension and topothesy varying with the mean separation of two contact surfaces. J Tribol 2006;128:515–24.
[49] Chung JC, Lin JF. Variation in fractal properties and non-Gaussian distributions of microcontact between elastic-plastic rough surfaces with mean surface separation. J Appl Mech 2006;73:143–52.
[50] Almqvist N. Fractal analysis of scanning probe microscopy images. Surf Sci 1996;355:221–8.
[51] Mandelbrot BB, Passoja DE, Paullay AJ. Fractal character of fracture surfaces of metals. Nature 1984;308:5961.
[52] Jiang S, Zheng Y, Zhu H. A contact stiffness model of machined plane joint based on fractal theory. J Tribol 2010;132:011401.
[53] Gelli N, Bobji M, Mohan S. Effect of contact stresses on shape recovery of niticu thin films. Thin Solid Films; 2014.
[54] Uchic MD, Shade PA, Dimiduk DM. Plasticity of micrometer-scale single crystals in compression. Annu Rev Mater Res 2009;39:361–86.
[55] Liu P, Zhao H, Huang K, Chen Q. Research on normal contact stiffness of rough surface considering friction based on fractal theory. Appl Surf Sci 2015;349:43–8.
[56] Kogut L, Komvopoulos K. Electrical contact resistance theory for conductive rough surfaces. J Appl Phys 2003;94:3153–62.
[57] Vallet C, Lasseux D, Sainsot P, Zahouani H. Real versus synthesized fractal surfaces: Contact mechanics and transport properties. Tribol Int 2009;42:250–9.
[58] Warren TL, Krajcinovic D. Fractal models of elastic-perfectly plastic contact of rough surfaces based on the Cantor set. Int J Solids Struct 1995;32:2907–22.
[59] Warren T, Majumdar A, Krajcinovic D. A fractal model for the rigid-perfectly plastic contact of rough surfaces. J Appl Mech 1996;63:47–54.
[60] Barber J. Bounds on the electrical resistance between contacting elastic rough bodies. In: Proceedings of the royal society of London. Series A: mathematical, physical and engineering sciences, 459; 2003. p. 53–66.
[61] Zhai C, Hanaor D, Proust G, Brassart L, Gan Y. Interfacial electro-mechanical behaviour at rough surfaces. Extr Mech Lett 2016.
[62] Akarapu S, Sharp T, Robbins MO. Stiffness of contacts between rough surfaces. Phys Rev Lett 2011;106:204301.
[63] Gonzalez-Valadez M, Baltazar A, Dwyer-Joyce R. Study of interfacial stiffness ratio of a rough surface in contact using a spring model. Wear 2010;268:373–9.
[64] Pastewka L, Prodanov N, Lorenz B, Müser MH, Robbins MO, Persson BN. Finite–size scaling in the interfacial stiffness of rough elastic contacts. Phys Rev E 2013;87:062809.
[65] Sneddon IN. The relation between load and penetration in the axisymmetric Boussinesq problem for a punch of arbitrary profile. Int J Eng Sci 1965;3:47–57.
[66] Oliver WC, Pharr GM. Measurement of hardness and elastic modulus by instrumented indentation: advances in understanding and refinements to methodology. J Mater Res 2004;19:3–20.
[67] Pharr G, Oliver W, Brotzen F. On the generality of the relationship among contact stiffness, contact area, and elastic modulus during indentation. J Mater Res 1992;7:613–17.
[68] McFarlane J, Tabor D. Relation between friction and adhesion. In: Proceedings of the royal society of London A: mathematical, physical and engineering sciences. The Royal Society; 1950. p. 244–53.
[69] Clarke KC. Computation of the fractal dimension of topographic surfaces using the triangular prism surface area method. Comput Geosci 1986;12:713–22.
[70] Douketis C, Wang Z, Haslett TL, Moskovits M. Fractal character of cold-deposited silver films determined by low-temperature scanning tunneling microscopy. Phys Rev B 1995;51:11022.
[71] Zahn W, Zösch A. The dependence of fractal dimension on measuring conditions of scanning probe microscopy. Fresenius J Anal Chem 1999;365:168–72.
[72] De Santis A, Fedi M, Quarta T. A revisitation of the triangular prism surface area method for estimating the fractal dimension of fractal surfaces. Ann Geophys 1997;40:811–21.
[73] Sarkar N, Chaudhuri B. An efficient differential box-counting approach to compute fractal dimension of image. Syst Man Cybern IEEE Trans 1994;24:115–20.
[74] Xie H, Wang J-a, Stein E. Direct fractal measurement and multifractal properties of fracture surfaces. Phys Lett A 1998;242:41–50.
[75] Zhai C, Hanaor D, Proust G, Gan Y. Stress-dependent frequency response of conductive granular materials. In: 2016 IEEE 62th holm conference on electrical contacts. IEEE; 2016. p. 9–16.
[76] Zhai C, Hanaor D, Proust G, Gan Y. Stress-dependent electrical contact resistance at fractal rough surfaces. J Eng Mech 2015:B4015001.
[77] Qiu D, Peng L, Yi P, Lai X. A micro contact model for electrical contact resistance prediction between roughness surface and carbon fiber paper. Int J Mech Sci 2017;124:37–47.
[78] Ciavarella M, Xu Y, Jackson RL. Some closed form results for adhesive rough contacts near complete contact on loading and unloading in the JKR regime. J Tribol 2017.
[79] Bahrami M, Culham J, Yovanovich MM, Schneider G. Thermal contact resistance of nonconforming rough surfaces, part 1: contact mechanics model. J Thermophys Heat Transfer 2004;18:209–17.
[80] Mulvihill D, Brunskill H, Kartal M, Dwyer-Joyce R, Nowell D. A comparison of contact stiffness measurements obtained by the digital image correlation and ultrasound techniques. Exp Mech 2013;53:1245–63.
[81] Pullen J, Williamson J. On the plastic contact of rough surfaces. In: Proceedings of the royal society of London A: mathematical, physical and engineering sciences. The Royal Society; 1972. p. 159–73.